Flux pinning evolution in multilayer Pb/Ge/Pb/Ge/Pb superconducting systems

Li-Xin Gao(高礼鑫)[1], Xiao-Ke Zhang(张晓珂)[1], An-Lei Zhang(张安蕾)[1], Qi-Ling Xiao(肖祁陵)[1], Fei Chen(陈飞)[1], and Jun-Yi Ge(葛军怡)[1,2,3,†]

[1] *Materials Genome Institute, Shanghai University, Shanghai* 200444, *China*
[2] *Shanghai Key Laboratory for High Temperature Superconductors, Shanghai University, Shanghai* 200444, *China*
[3] *Zhejiang Laboratory, Hangzhou* 311100, *China*

(Received 22 April 2022; revised manuscript received 20 July 2022; accepted manuscript online 16 August 2022)

Multicomponent superconductors exhibit nontrivial vortex behaviors due to the various vortex–vortex interactions, including the competing one in the recently proposed type-1.5 superconductor. However, potential candidate that can be used to study the multicomponent superconductivity is rare. Here, we prepared an artificial superconducting multilayer to act as an alternative approach to study multicomponent superconductivity. The additional repulsive length and the coupling strength among superconducting films were regulated by changing the thickness of the insulting layer. The magnetization measurements were performed to clarify the effect of the competition between the repulsive vortex interactions on the macroscopic superconductivity. The vortex phase diagram and the optimum critical current density have been determined. Furthermore, a second magnetization effect is observed, and is attributed to the upper layer, which provides the weak pinning sites to localize the flux lines. The pinning behaviors switches to the mixed type with the increase of the insulting layer thicknesses. Our results open a new perspective to the study and related applications of the multilayer superconducting systems.

Keywords: multilayer superconducting film, competing interaction, flux pinning mechanism

PACS: 74.25.Ha, 74.25.Dw, 74.25.Bt, 74.25.op **DOI:** 10.1088/1674-1056/ac89e1

Competing interactions favor spatial inhomogeneities in an otherwise uniform ground state have been found in many systems including superconductors,[1–3] ferrofluids,[4] ferromagnetic films,[5] and organic systems,[6] among which the vortex matter in different kinds of superconductors provides a unique platform to study the complex interactions and their manifestations.

Generally, superconductors are divided into two categories using the Ginzburg–Landau (GL) parameter $\kappa = \lambda/\xi$, where λ is the magnetic penetration length and ξ is the coherence length. In type-1 superconductors with $\kappa < 1/\sqrt{2}$, the positive superconducting/normal interface energy favors an attractive vortex–vortex (vv) interaction, leading to the formation of intermediate state with coexistence of normal and superconducting domains inside the superconductor.[7,8] In type-2 superconductors with $\kappa > 1/\sqrt{2}$, the interface energy becomes negative and the vv interaction is purely repulsive, resulting in the formation of mixed state with triangular vortex lattice, also known as Abrikosov vortex lattice.[9] In 2005, it is proposed that, in multiband superconductors, a non-monotonic vv interaction can occur when $\xi_1 < \lambda < \xi_2$, where ξ_1 and ξ_2 are the coherence lengths of different condensates.[10] As a result, the semi-Meissner state with exotic vortex patterns, such as vortex cluster, vortex stripe, and vortex-free area, are expected. Later, this new vortex state was confirmed experimentally by mapping the vortex patterns in the two-band superconductor MgB_2 single crystal.[11] This novel superconducting state, which cannot be interpreted by the above mentioned dichotomy, was termed as type-1.5 superconductivity. The discovery of this unconventional superconductor has attracted great interests in condensed matter physics because it provides an excellent platform to study the phenomenon resulted from competing interactions.[12,13] However, so far only a limited number of two-band or multi-band superconductor have been found to fall into this category.[11,14]

An alternative approach to study multicomponent superconducting systems using artificial multilayer films was proposed.[15,16] Rich vortex phases were predicted in multilayer superconducting structures, where the properties of each layer and their coupling can be easily tuned by changing the characteristic lengths and the interlayer distance.[16] Experimentally, an unconventional temperature dependence of critical fields, which is consistent with a multicomponent system, was reported in Nb/Pb/Nb trilayer with spatially separated superconducting films.[17] Further theoretical study have shown that, in multilayer systems, it is not necessary for the superconducting layers to locate at opposite sides of the Bogomolnyi point $\kappa = 1/\sqrt{2}$. Combining two components with both repulsive vv interactions can also lead to a competing interaction.[18] Up to now, the research on multilayer super-

†Corresponding author. E-mail: junyi_ge@t.shu.edu.cn
© 2023 Chinese Physical Society and IOP Publishing Ltd

conducting system is mainly limited to theoretical simulations, while the experimental studies are rare. Meanwhile, it is necessary to clarify how the transitions of the vortex phases are manifested in the macroscopic superconductivity.

In this paper, the conventional Pb films were chosen as the unit superconducting layer to design a multilayer superconducting system by separating with an insulating layer. The macroscopic phenomena, resulting from intricate vv interactions, as a function of the insulating layer thickness, are studied. It is found that a weak second magnetization peak (SMP) appears due to the weak pinning centers which are provided from the upper layer. The flux pinning evolution and the disappearance of SMP are discovered with the increase of the insulating layer thicknesses. In addition, the varieties of the critical current density have been observed, which is beneficial to find out the optimum parameters for practical applications in multilayer superconducting films.

The superconducting unit layer Pb film of 100-nm thickness was prepared by electron beam evaporation on SiO_2/Si substrate. During deposition, the substrates were cooled to -150 °C by liquid nitrogen. The pressure of the deposition chamber was maintained at 2×10^{-3} Pa and the deposition rate is fixed at 1 Å/s during evaporation. Between two unit layers, Ge layers with the thicknesses of 10 nm, 20 nm, 50 nm, and 100 nm were grew as insulating layers. After repeating the above steps, the final Pb/Ge/Pb/Ge/Pb multilayer structures were obtained. To protect the surface from oxidation, all multilayer films were finally capped with a 10-nm thick Ge layer. In the following discussion, the multilayer samples with the insulating layer thicknesses of 10 nm, 20 nm, 50 nm, and 100 nm are defined as S1, S2, S3, and S4, respectively. All samples were cut into 2 mm × 2 mm for dc magnetization measurements.

The surface morphology was checked in the tapping mode by using an atomic force microscope (AFM). The magnetization measurements were performed using a magnetic property measurement system (MPMS, Quantum Design) with the external magnetic field applied perpendicular to the films.

For a conventional type-2 superconducting film, vortices are expected to form a triangular lattice due to the pure repulsive vv interactions, as shown in Fig. 1(a). When combining superconducting films to construct the multilayer structure in Fig. 1(b), the vortices in each superconducting layer will experience the interaction in adjacent layers. Theoretically, this may result in rather intricate vv interactions, including the competing one. Nontrivial vortex patterns, such as vortex strips and clusters (Fig. 1(c)), could form. In Pb/Ge/Pb/Ge/Pb multilayer, the flux spreads in non-superconducting regions as shown in Fig. 1(b). The additional repulsive length appears due to the wider spread of the magnetic field lines by increasing the thickness of insulating layers in this paper. The coupling strength among superconducting films and the additional repulsive length were regulated by increasing the thickness of Ge films.

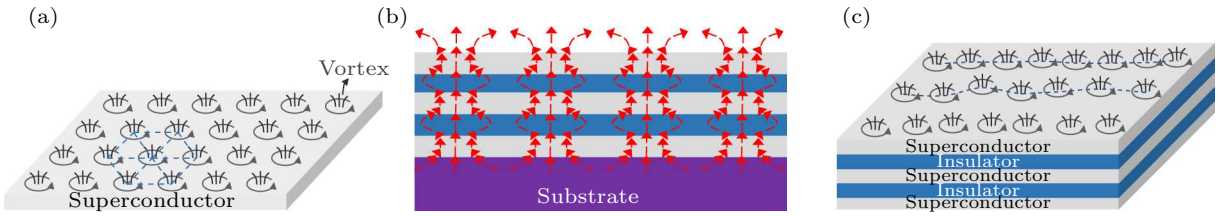


Fig. 1. (a) The schematic vortex configurations in Pb monolayer films of 100-nm thickness. (b) The flux lines in the multilayer superconducting system. Grey (blue) areas are Pb (Ge) layers. (c) The unconventional vortex stripe phases arise from purely repulsive interactions.

First, we characterize the suprconducting properties of an individual superconducting layer. Figure 2(a) shows the topography of the studied Pb monolayer of 100 nm. The compact grains and flat surface with a roughness of 1.2 nm indicate the high quality of the film. The isothermal magnetization loops were measured at different temperatures, ranging from 2 K to 7 K, as shown in Fig. 2(b). The critical current density J_c was calculated by using the M–H curves according to the Bean critical state model[19–21] in Fig. 2(c). The used formula[22] is shown as follows: $J_c = (20\Delta M)/(a(1-a/3b))$, where $\Delta M = M_{down} - M_{up}$, with M_{down} and M_{up} being the magnetizations when sweeping fields down and up, respectively. Here, a and b are the sample width and length ($a < b$). The results of J_c at 7 K were neglected because of the faint magnetization. The pinning force density F_p are obtained by using the relation $F_p = \mu_0 H \times J_c$ to figure out the pinning mechanism of the film. The curves of the reduced pinning force f *versus* the reduced magnetic field h ($f = F_p/F_{pmax}$, F_{pmax} standing for the maximum of the pinning force, $h = H/H_{c2}$) are presented in Fig. 2(d). According to the Dew–Hughes model,[23,24] the reduced field h dependence of the normalized pinning force density f measured at different temperatures should obey the general relationship that f is proportional to $h^p(1-h)^q$ in case of existence of a single dominant pinning mechanism, where p and q depend on the mechanism of pinning. In general, the grain boundary pinning plays a major role when p (q) is close to 0.5 (2), while the non-superconducting point pinning becomes mainly responsible with $p = 1$ ($q = 2$).

The experimental data were fitted well with $p = 0.73$ and $q = 1.61$. The position of the maximum of the pinning force $h_{max} = p/(p+q) \approx 0.31$ slight deviates from point pinning ($h_{max}^{fit} = 0.33$). Therefore, we suggest that the point pinning and grain boundary pinning work together in the Pb monolayer film.

As is known, the critical current density J_c can act as a suitable parameter to gain more insight to the underlying pinning mechanism according to the collective pinning theory.[25] The disorder-induced spatial fluctuations in the vortex lattice can be explicitly divided into different regimes with the increase of the external fields: single-vortex pinning, small-bundle pinning, large-bundle pinning, and charge-density-wave-type relaxation of the vortex lattice to the disorder potential. The crossover field from the single-vortex pinning regime to the small-bundle pinning regime is defined as B_{sb}. Theoretically, the interaction between vortices is irrelevant and J_c is independent of the field in the regime below B_{sb}. However, the dc magnetization only gives an estimate of J_c and, to some extent, it yields a relaxed value of $J(t) \leq J_c$. The relaxation effects, caused by the vortices creeping out of the dense random pinning wells, affect $M(H)$ at all temperatures.[26] Therefore, at low fields the observed J_c is determined by the collective creep, while at high fields (the bundle pinning regime) the pinning energy is large, hence the relaxation is small and the field dependence of J_c is essentially determined by $J_c(B)$.[27] With the applied field above the crossover field B_{sb}, $J_c(B)$ follows an exponential law: $J_c(B) \approx J_c(0)\exp -(B/B_0)^{3/2}$, where B_0 represents a normalization parameter on the order of B_{sb}. The normalized J_c in a double logarithmic plot of $-\log[J_c(B)/J_c(0)]$ as a function of field is plotted in Fig. 2(e). The deviation point in the linear fitting at the lower field is denoted as B_{sb}, while the deviation point B_{th} at the upper field is connected to large thermal fluctuations.[28] The temperature dependence of the crossover field B_{sb}, which reflects the pinning behaviors, can be expressed as:[29,30] $B_{sb} = B_{sb}(0)[(1-t^2)/(1+t^2)]^v$, where $v = 2/3$ and 2 stands for δT_c and δl pinning, respectively. The pinning behavior which is called δT_c pinning results from the spatial variations of the Ginzburg–Landau (GL) coefficient α in connection with fluctuations in the transition temperature T_c. The spatial fluctuations in the charge carrier mean free path l near the lattice defects which pin the flux lines lead to δl pinning.[31–34] Figure 2(f) displays the scaled experimental data B_{sb} with the theoretically calculated δT_c and δl pinning (solid lines). It can be seen that the pinning mechanism of the Pb monolayer film consists of both above behaviors and δT_c pinning plays a major role.

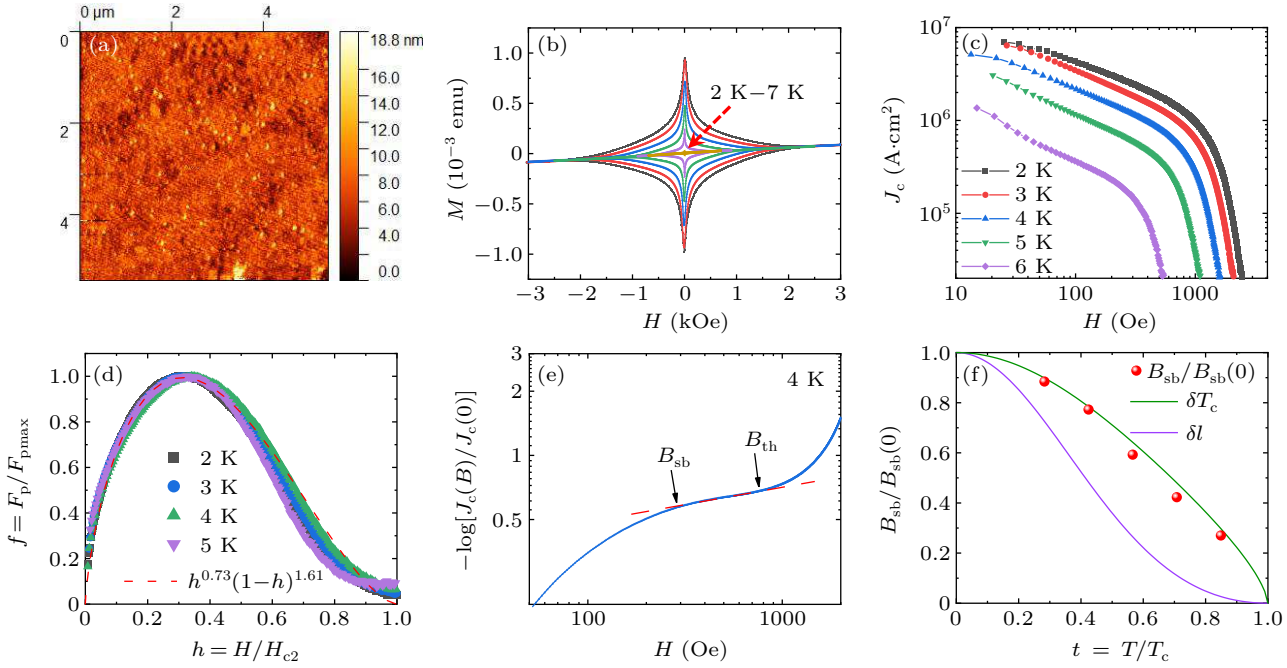


Fig. 2. (a) The AFM image showing the surface topography of the Pb monolayer film. (b) The isothermal magnetization loops measured at various temperatures. (c) Critical current (J_c) *versus* magnetic field (H) in a double logarithmic plot. (d) The rescaled density of the pinning force as a function of the reduced field, $h = H/H_{c2}$. (e) Critical current (J_c) *versus* magnetic field (H) in a double logarithmic plot as $-\log(J_c/J_c(B=0))$ *versus* $\log H$. The solid lines are the linear fit to the data. (f) Plots of $B_{sb}/B_{sb}(0)$ *versus* T/T_c. The green and purple lines represent the theoretical curves for δT_c pinning and the δl pinning, respectively. The unit 1 Oe = 79.5775 A·m^{-1}.

Figures 3(a)–3(d) show the isothermal magnetization loops measured at various temperatures for S1 (a), S2 (b), S3 (c), and S4 (d). A weak second magnetization peak is observed only in S1 in the temperature range of 2 K–6 K. The occurrence of SMP has been observed in both superconducting films[35] and single crystals. The shoulder-like phenomenon observed for our multilayer sample is rather similar to that reported in $BaFe_{1.8}Co_{0.2}As_2$ and $Ca_{0.8}La_{0.2}Fe_{1-x}Co_xAs_2$ [36,37]

single crystals. Among the various theoretical models, the crossover from elastic to plastic (EP) vortex creep is widely adopted.[38] At the relatively low field, vortices are well separated and act like non-interacting objects, which makes flux lines tend to be captured by strong pinning centers. Near the EP crossover region, the number of vortices is larger than the strong pinning centers, and the extra vortices better adjust to the weak collective pinning centers which are produced by the softening of elastic vortices. The additional effective pinning centers lead to the increase of pinning force and critical current density J_c, while the weak elementary pinning force of individual pinning center reduces the sum of elementary pinning force and J_c. The SMP only appears when the increase of J_c caused by the former exceeds the reduction of the sum of elementary pinning force. Therefore, the increase of the pinning strength benefited from additional pinning centers leads to the occurrence of SMP in S1. As the insulting layer thicknesses increase, the additional repulsions reduce the sum of elementary pinning force, resulting in the disappearance of SMP. For the Pb monolayer film, the grain boundaries provide the effective pinning centers to capture the flux lines which suppresses the SMP. Figures 3(e)–3(h) present the critical current density (J_c) *versus* magnetic field (H) in a double logarithmic plot ranging from 2 K to 6 K for S1 (e), S2 (f), S3 (g), and S4 (h). The shoulder in Fig. 3(e) corresponds to the SMP on the isothermal magnetization loop of S1. The SMP is shifted to low fields as the temperature increases.

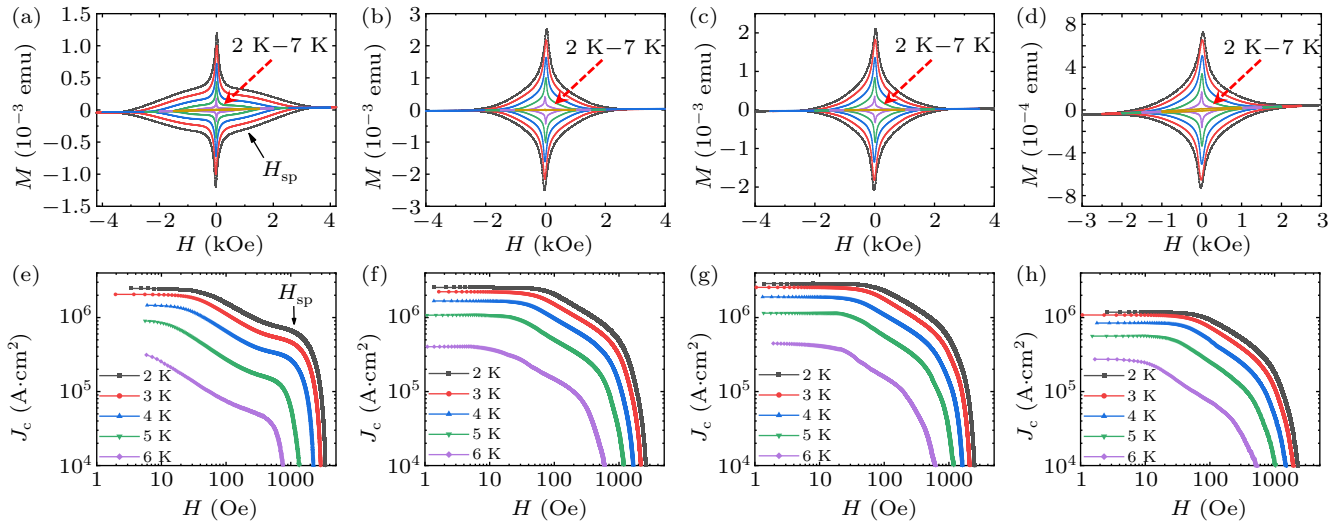


Fig. 3. (a)–(d) The isothermal magnetization loops measured at various temperatures for S1 (a), S2 (b), S3 (c), and S4 (d), respectively. (e)–(h) Critical current density (J_c) *versus* magnetic field (H) in a double logarithmic plot ranging from 2 K to 6 K for S1 (e), S2 (f), S3 (g), and S4 (h).

The vortex phase diagram of S1 is shown in Fig. 4(a). The vortex liquid state is ignored because the irreversible field (H_{irr}) is quite close to the critical field (H_{c2}) for Pb. The transition points (H_{sp}) from the elastic vortex glass state to the plastic vortex glass state are obtained according to the isothermal magnetization loops. As usual, the SMP shifts to lower fields as the temperature increases.[39,40] The temperature dependence of the critical fields of all samples are shown in Fig. 4(b). Furthermore, the critical fields with the change of Ge thicknesses are presented in Fig. 4(c). It is known that, by introducing defects into conventional superconductors, H_{c2} can be improved.[41,42] For the monolayer Pb film, the growth of the granular film is continuous, the connection of the grains is compact. Therefore, the number of defects is expected be small. However, for the multilayer Pb films, the introduction of a thin Ge layer (10 nm) separates the superconducting Pb films. As a result, more defects are expected to appear in the upper layer films, resulting in a decrease of the coherence length, *i.e.*, an increase of the upper critical magnetic field. This can also be supported by the fact that, the roughness becomes larger in the multilayer film. The critical current density (J_c) of Pb multilayer films at $T = 4$ K and $H = 100$ Oe are demonstrated in Fig. 4(c). The value of critical current density J_c shows a trend of increasing first and then decreasing. The grain boundaries in S2 act as the strong pinning centers leading to a larger critical current density than S1. We suggest that, with increasing the insulating layer thicknesses, the critical current density decreases due to the more prominent vortex–vortex repulsive interactions to overcome the pinning force. This result implies that it is feasible to regulate the optimum critical current density by adjusting the thickness of the insulating layer, which provide valuable insights into the potential applications for multilayer superconducting films.

In order to clarify the effect of the competition between the repulsive vortex interactions on the macroscopic superconductivity of Pb multilayer films, the pinning behaviors are acquired according to J_c by using the methods mentioned above as shown in Fig. 5. The fitting based on the scaling functions

leads to $p = 1.39$ and $q = 1.70$ with position of the maximum of the pinning force $h_{max} \approx 0.45$ for S1 in Fig. 5(a). This result is very close to that in $BaFe_{1.8}Co_{0.2}As_2$ ($h \sim 0.45$) and $Ca_{0.8}La_{0.2}Fe_{1-x}Co_xAs_2$ ($h \sim 0.45$).[36,37] Such h value was considered to be an indication of dense vortex pinning nanostructures or weak pinning sites.[43] In this paper, the random distributed nano-scale point-like defects which caused by the dense small grains provide the weak pinning sites. Moreover, the plenty of the weak pinning centers is helpful for the pinning energy of additional pinning centers to overcome the change of the elastic energy of flux lines. In this case, EP crossover will occur and induce SMP. The exotic-element-doped and irradiation technique are adopted to introduce the large set of weak pinning centers, resulting in the emergence of SMP.[44–48] Therefore, we suggest that the upper layer provides the weak pinning sites corresponding to viewpoint proposed by Babaev[49] to localize the flux lines, which leads to the appearance of SMP. Meanwhile, the pinning mechanism of S1 is δT_c pinning. With the increase of the insulating layer thicknesses, the pinning behaviors switches to the mixed type and the grain boundary pinning gradually play a major role. The flux lines are more likely captured in strong pinning centers with large sizes because the weakening of coupling strength and the appearance of the additional repulsive length. At present, the mean free path can be greatly influenced by the gain-boundary-like behavior, which results in the shift from δT_c pinning to δl pinning.[50] Furthermore, the evolution of pinning properties can provide valuable insights into the study and related applications of the multilayer superconducting films.

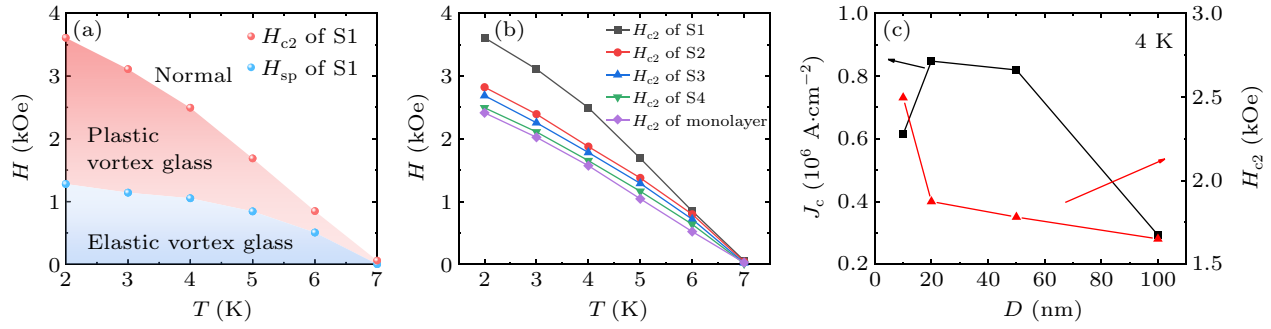


Fig. 4. (a) Vortex phase diagram of S1. (b) Temperature dependence of upper critical field (H_{c2}) of all samples ranging from 2 K to 7 K. (c) Critical current density (J_c) and upper critical field (H_{c2}) with the change of Ge thicknesses for Pb multilayer films at $T = 4$ K.

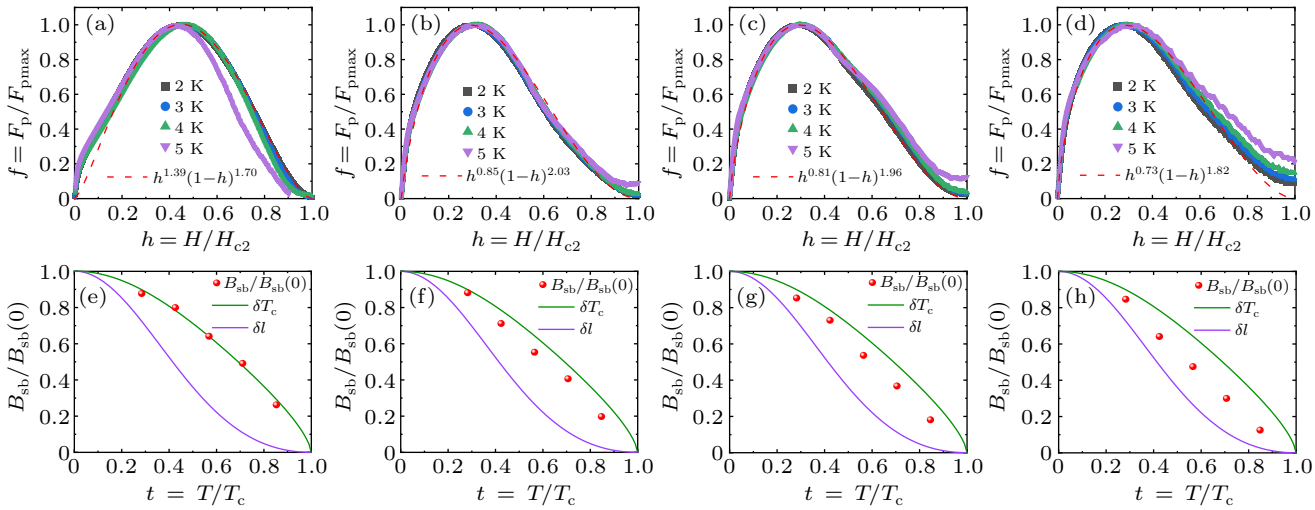


Fig. 5. (a)–(d) The rescaled density of the pinning force as a function of the reduced field for S1 (a), S2 (b), S3 (c), and S4 (d), respectively. (e)–(f) Plots of $B_{sb}/B_{sb}(0)$ *versus* T/T_c for S1 (e), S2 (f), S3 (g), and S4 (h).

In conclusion, we have prepared a multilayer superconducting system. By varying the insulating layer thickness to tune the coupling strength between superconducting layers, the superconducting properties and the flux pinning evolution was studied. The vortex phase diagram consisted of all samples has been determined. The critical field of multilayer films becomes smaller when the thicknesses of Ge layers increase. Meanwhile, it is feasible to regulate the optimum critical current density by adjusting the thickness of the insulating layer. Furthermore, the upper layer provides the weak pinning sites to localize the flux lines resulting in the appearance of SMP. The pinning behaviors switches to the mixed type with the weakening of coupling strength and the appearance of the additional repulsive length. Our results provide a new perspective to study the connection between macro superconductivity and micro repulsive interactions in multilayer superconducting

system.

Acknowledgments

Project supported by the National Natural Science Foundation of China (Grant No. 12174242), the National Key Research and Development Program of China (Grant No. 2018YFA0704300), the Key Research Project of Zhejiang Laboratory (Grant No. 2021PE0AC02). Jun-Yi Ge also thanks the support by the Program for Professor of Special Appointment (Eastern Scholar) at Shanghai Institutions of Higher Learning.

References

[1] Brandt E H and Das M P 1995 *Rep. Prog. Phys.* **58** 1465
[2] Ge J Y, Gutierrez J, Lyashchenko A, Filipov V, Li J and Moshchalkov V V 2014 *Phys. Rev. B* **90** 184511
[3] Reimann T, Mühlbauer S, Schulz M, Betz B, Kaestner A, Pipich V, Böni P and Grünzweig C 2015 *Nat. Commun.* **6** 8813
[4] Bacri J C and Salin D 1988 *Endeavor* **12** 76
[5] Seul M and Andelman D 1995 *Science* **267** 476
[6] Weis R M and McConnell H M 1984 *Nature* **310** 47
[7] Kramer L 1971 *Phys. Rev. B* **3** 3821
[8] Brandt E H 1986 *Phys. Rev. B* **34** 6514
[9] Abrikosov A A 1957 *Zh. Eksp. Teor. Fiz.* **32** 1442
[10] Babaev E and Speight M 2005 *Phys. Rev. B* **72** 180502
[11] Moshchalko V V, Menghini M, Nishio T, Chen Q H, Silhanek A V, Dao V H, Chibotaru L F, Zhigadlo N D and Karpinski J 2009 *Phys. Rev. Lett.* **102** 117001
[12] Backs A, Schulz M, Pipich V, Kleinhans M, Böni P and Mühlbauer S 2019 *Phys. Rev. B* **100** 064503
[13] Vagov A, Wolf S, Croitoru M D and Shanenko A A 2020 *Commun. Phys.* **3** 58
[14] Garaud J, Agterberg D F and Babaev E 2012 *Phys. Rev. B* **86** 060513
[15] Komendova L, Milosevic M V and Peeters F M 2013 *Phys. Rev. B* **88** 094515
[16] Varney C N, Sellin K A H, Wang Q Z, Fangohr H and Babaev E 2013 *J. Phys.: Condens. Matter.* **25** 415702
[17] Portela F S, Corredor L T, Barrozo P, Jung S, Zhang G, Vanacken J, Moshchalkov V V and Aguiar J A 2015 *Supercond. Sci. Technol.* **28** 034001
[18] Malescio G and Pellicane G 2003 *Nat. Mater.* **2** 97
[19] Bean C P 1964 *Rev. Mod. Phys.* **36** 31
[20] Shi Z X, Ji H L, Zhang Y T, Jin X, Xu X N, Ding S Y, Yao X X, Wang C A, Wang R L, Li H C, Zhang H, Sun Z J and Yang Z S 1994 *Chin. Phys. B* **3** 124
[21] Feng Y, Zhou L, Shi L, Yang W M, Zhang C P, Wang J R, Du Z H, Yu Z M, Wu X Z and Zhang Y H 1999 *Chin. Phys. B* **8** 374
[22] Ishida S, Iyo A, Ogino H, Eisaki H, Takeshita N, Kawashima K, Yanagisawa K, Kobayashi Y, Kimoto K, Abe H, Imai M, Shimoyama J and Eisterer M 2019 *Npj Quantum Mater.* **4** 27
[23] Dew-Hughes D 1974 *Philos. Mag.* **30** 293
[24] Dew-Hughes D 1987 *Philos. Mag. B* **55** 459
[25] Blatter G, Feigel'man M V, Geshkenbein V B, Larkin A I and Vinokur V M 1994 *Rev. Mod. Phys.* **66** 1125
[26] Malozemoff A P and Fisher M P A 1990 *Phys. Rev. B* **42** 6784
[27] Krusin-Elbaum L, Civale L, Vinokur V M and Holtzberg F 1992 *Phys. Rev. Lett.* **69** 2280
[28] Ghorbani S R, Wang X L, Dou S X, Lee S I K and Hossain M S A 2008 *Phys. Rev. B* **78** 184502
[29] Griessen R, Wen H H, van Dalen A J J, Dam B, Rector J, Schnack H G, Libbrecht S, Osquiguil E and Bruynseraede Y 1994 *Phys. Rev. Lett.* **72** 1910
[30] Qin M J, Wang X L, Liu H K and Dou S X 2002 *Phys. Rev. B* **65** 132508
[31] Thuneberg E V, Kurkijärvi J and Rainer D 1982 *Phys. Rev. Lett.* **48** 1853
[32] Thuneberg E V 1989 *Cryogenics.* **29** 236
[33] van der Beck C J and Kes P H 1991 *Phys. Rev. B* **43** 13032
[34] Kes P H 1991 *Physica C* **185–189** 288
[35] Aliev A E, Lee S B, Zakhidov A A and Baughman R H 2007 *Physica C* **453** 15
[36] Yamamoto A, Jaroszynski J, Tarantini C, Balicas L, Jiang J, Gurevich A, Larbalestier D C, Jin R, Sefat A S, McGuire M A, Sales B C, Christen D K and Mandrus D 2009 *Appl. Phys. Lett.* **94** 062511
[37] Zhou W, Xing X Z, Wu W J, Zhao H J and Shi Z X 2016 *Sci. Rep.* **6** 22278
[38] Abulafia Y, Shaulov A, Wolfus Y, Prozorov R, Burlachkov L and Yeshurun Y 1996 *Phys. Rev. Lett.* **77** 1596
[39] Yang H, Luo H, Wang Z and Wen H H 2008 *Appl. Phys. Lett.* **93** 142506
[40] Galluzzi A, Buchkov K, Tomov V, Nazarova E, Leo A, Grimaldi G, Nigro A, Pace S and Polichetti M 2018 *Supercond. Sci. Technol.* **31** 015014
[41] Cooley L D, Hu Y F and Moodenbaugh A R 2006 *Appl. Phys. Lett.* **88** 142506
[42] Baumgartner T, Eisterer M, Weber H W, Flükiger R, Scheuerlein C and Bottura L 2014 *Supercond. Sci. Technol.* **27** 015005
[43] Sun D L, Liu Y and Lin C T 2009 *Phys. Rev. B* **80** 144515
[44] Küpfer H, Wolf Th, Lessing C, Zhukov A A, Lançon X, Meier-Hirmer R, Schauer W and Wühl H 1998 *Phys. Rev. B* **58** 2886
[45] Prozorov R, Ni N, Tanatar M A, Kogan V G, Gordon R T, MartinC, Blomberg E C, Prommapan P, Yan J Q, Bud'ko S L and Canfield P C 2008 *Phys. Rev. B* **78** 224506
[46] Salem-Sugui S, Ghivelder Jr L, Alvarenga A D, Cohen L F, Yates K A, Morrison K, Pimentel J L, Huiqian Luo Jr, Wang Z S and Wen H H 2010 *Phys. Rev. B* **82** 054513
[47] Dongjoon S, Shigeyuki I, Akira I, Masamichi N, Jun-ichi S, Michael E and Hiroshi E 2016 *Sci. Rep.* **6** 26671
[48] Mishev V, Nakajima M, Eisaki H and Eisterer M 2016 *Sci. Rep.* **6** 27783
[49] Meng Q Y, Varney C N, Fangohr H and Babaev E 2014 *Phys. Rev. B* **90** 020509
[50] Zhang A L, Jiang W Y, Chen X H, Zhang X K, Lu W L, Chen F, Feng Z J, Cao S X, Zhang J C and Ge J Y 2022 *Curr. Appl. Phys.* **35** 32